The Journal of Chemical Physics

Quantum dynamics of hydrogen atoms on graphene. II. Sticking

Cite as: J. Chem. Phys. **143**, 124704 (2015); https://doi.org/10.1063/1.4931117
Submitted: 22 July 2015 • Accepted: 04 September 2015 • Published Online: 23 September 2015

Matteo Bonfanti, Bret Jackson, Keith H. Hughes, et al.

Quantum dynamics of hydrogen atoms on graphene. II. Sticking

Matteo Bonfanti,[1,a)] Bret Jackson,[2] Keith H. Hughes,[3] Irene Burghardt,[4] and Rocco Martinazzo[1,5,b)]

[1]*Dipartimento di Chimica, Università degli Studi di Milano, v. Golgi 19, 20133 Milano, Italy*
[2]*Department of Chemistry, University of Massachusetts, Amherst, Massachusetts 01003, USA*
[3]*School of Chemistry, Bangor University, Bangor, Gwynedd LL57 2UW, United Kingdom*
[4]*Institute of Physical and Theoretical Chemistry, Goethe University Frankfurt, Max-von-Laue-Str. 7, 60438 Frankfurt/Main, Germany*
[5]*Istituto di Scienze e Tecnologie Molecolari, Consiglio Nazionale delle Richerche, v. Golgi 19, 20133 Milano, Italy*

(Received 22 July 2015; accepted 4 September 2015; published online 23 September 2015)

Following our recent system-bath modeling of the interaction between a hydrogen atom and a graphene surface [Bonfanti *et al.*, J. Chem. Phys. **143**, 124703 (2015)], we present the results of converged quantum scattering calculations on the activated sticking dynamics. The focus of this study is the collinear scattering on a surface at zero temperature, which is treated with high-dimensional wavepacket propagations with the multi-configuration time-dependent Hartree method. At low collision energies, barrier-crossing dominates the sticking and any projectile that overcomes the barrier gets trapped in the chemisorption well. However, at high collision energies, energy transfer to the surface is a limiting factor, and fast H atoms hardly dissipate their excess energy and stick on the surface. As a consequence, the sticking coefficient is maximum (~0.65) at an energy which is about one and half larger than the barrier height. Comparison of the results with classical and quasi-classical calculations shows that quantum fluctuations of the lattice play a primary role in the dynamics. A simple impulsive model describing the collision of a *classical* projectile with a *quantum* surface is developed which reproduces the quantum results remarkably well for all but the lowest energies, thereby capturing the essential physics of the activated sticking dynamics investigated. © *2015 AIP Publishing LLC.* [http://dx.doi.org/10.1063/1.4931117]

I. INTRODUCTION

Adsorption of hydrogen atoms to graphite and graphenic surfaces is one of the simplest and most studied processes in surface science. Hydrogenation of graphite was first considered, both theoretically[1,2] and experimentally,[3] for a fundamental interest: it is now well established that H_2 formation in the interstellar medium (ISM) involves the carbonaceous surface of the interstellar dust particles that acts as a "third body" in the collision process and allows the reaction partners to get rid of the excess energy of their recombination.[4–6] More recently, hydrogenation of graphenic surface has also attracted increased interest in applied physics since it has been argued that hydrogen adsorption could be a viable process to induce a reversible modulation of the electronic properties of graphene. Though experimental studies have shown adsorption-induced metal-insulator transitions,[7,8] reversible opening of a band-gap[9,10] and even ferromagnetic hysteresis,[11] the necessary precise control on the hydrogenation process has yet to be achieved. Hydrogenation of graphite has been studied in a number of experimental works,[3,12–24] with a variety of surface-science techniques including thermal desorption, high-resolution electron-energy-loss spectroscopy, scanning tunneling microscopy, low-energy electron diffraction, angle resolved photo-emission spectroscopy, and X-ray photoemission spectroscopy. It has now been well established that sticking is an activated process, with a barrier related to the surface reconstruction accompanying the $sp^2 \rightarrow sp^3$ re-hybridization of the carbon atom involved in the bond formation process.[3] As a consequence, carefully conducted scattering experiments which used low energy hydrogen atom beams — as opposed to high energy beams obtained by thermal cracking of H_2 — found that the competing, non-activated hydrogen abstraction process dominates under these conditions,[19] a result which was later confirmed by *ab initio* molecular dynamics simulations.[25] For all but the smallest coverage, hydrogenation is driven by electronic and substrate-softening effects which lead to dimer formation and clustering;[15,18,26,27] hence, current experimental results leave the question open of how large is the *initial* hydrogen sticking coefficient on the carbon sheet. Furthermore, a marked isotope effect has been found when hydrogenating epitaxial graphene grown on Au/Ni and it has been argued that it directly relates to the sticking cross sections.[23] More recently, the role of the specific graphenic substrate employed has been addressed, and substantial differences in hydrogen saturated structures have been reported between quasi-free-standing graphene and metal-bound graphene.[24]

At present, a complete and thorough description of this vast phenomenology is lacking, and experimental results, although pointing towards strong dynamical effects, are affected by such a large variety of almost uncontrollable factors

a)Electronic mail: matteo.bonfanti@unimi.it
b)Electronic mail: rocco.martinazzo@unimi.it

— the hydrogen coverage, the quality of the substrate, and the nature and energy distribution of the incident hydrogen atom beam — that they are all quite inconclusive for the very first adsorption events. This is rather unfortunate since in the rarefied and cold environment where much of the interstellar chemistry occurs hydrogenation hardly reaches the coverage conditions of typical terrestrial experiments, and thus likely proceeds in a rather different kinetic regime. Theory can be of great help in this context, since the extreme conditions mentioned above are ideal for theoretical modeling. To tackle such a problem from a theoretical perspective, a versatile and computationally feasible dynamical model is necessary. Many models have been proposed in the past, highlighting the many different effects, detailed below, that are needed to reach a quantitative description of the hydrogen sticking process:[28–35] (i) due to the fast substrate relaxation induced by the sp^2-sp^3 conversion, forces on the binding carbon atom are large and the motion of the latter is strongly coupled to the hydrogen coordinate;[28] (ii) a large fraction of the reaction takes place at the non-collinear geometries, since steering of the projectile is operative;[29] (iii) energy relaxation to graphene phonons is a relatively fast process and large amounts of energy need to be transferred that saturation effects are likely when truncating the phonon basis;[30,34] and (iv) quantum effects have large consequences on the sticking probability, particularly at the low collision energies of interest for the chemistry of the ISM where tunneling dominates.[29,32,33,35]

In the present paper, we investigate the sticking dynamics of a hydrogen atom on the clean graphene surface, using the system-bath model developed in a related paper,[51] henceforth denoted Paper I. The model accurately describes the hydrogen atom and its bonding carbon atom, includes a phonon bath mimicking the graphene substrate, and is numerically solvable with available, high-dimensional quantum dynamical methods, as has been already shown in Paper I where we addressed vibrational relaxation. The model relies on the density functional theory (DFT) potential energy surface (PES) of Ref. 36 and on an accurate force field of the lattice[36,37] which was mapped upon an independent oscillator (IO) bath. It describes explicitly the C-H "system," which is coupled to an "environment" through the carbon end only. Thus, the latter undergoes damped motion whose characteristic (state-independent) memory kernel was defined by means of an appropriate spectral density (SD) of the environmental coupling which was the main focus of Paper I. Here, we extend the dynamical investigations of the model to the case of main interest, by performing quantum scattering calculations in a dissipative setting.

The paper is organized as follows. In Section II, we give a brief description of the Hamiltonian model and of the PES adopted. In Section III, we discuss the methodology that we have used for computing sticking probabilities with both molecular dynamics and quantum dynamical simulations. In Section IV, we present and discuss the results, and then in Section V we summarize and conclude.

II. SYSTEM-BATH MODEL

The system-bath model developed in Paper I relies on the following IO Hamiltonian:

$$H = \frac{\mathbf{p}_H^2}{2m_H} + \frac{p_C^2}{2m_C} + V_s(\mathbf{x}_H, z_C) + \sum_{k=1}^{F}\left[\frac{p_k^2}{2m} + \frac{m\omega_k^2}{2}\left(q_k - \frac{c_k}{\omega_k^2}(z_C - z_C^{eq})\right)^2\right], \quad (1)$$

where $\mathbf{x}_H = (x_H, y_H, z_H)$ is the position of the H atom, z_C the height of the binding C atom above the surface, $m_H/\mathbf{p}_H$ and m_C/p_C are the corresponding mass/momenta, and m is a numerically convenient choice of the mass of the harmonic oscillators, whose position and momenta operators are denoted with q_k and p_k, respectively. $V_s(\mathbf{x}_H, z_C)$ is an appropriate 4D system potential which, consistently with the system-bath modeling, was defined to be

$$V_s(\mathbf{x}_H, z_C) = \underset{\{\mathbf{Q}\}}{\mathrm{Min}}\, V_{at}(\mathbf{x}_H, z_C, \mathbf{Q}), \quad (2)$$

where V_{at} is an accurate atomistic model of the H-graphene system[30] and $\mathbf{Q}$ is a set of lattice coordinates $\mathbf{Q} = \{Q_1, Q_2, ..Q_N\}$. In applying Eq. (1), the harmonic oscillators are given evenly spaced frequencies $\omega_k = k\Delta\omega$ and the coupling coefficients c_k are chosen to sample a SD $J_C(\omega)$,

$$c_k = \sqrt{\frac{2\, m\, \omega_k\, \Delta\omega\, J_C(\omega_k)}{\pi}}$$

which encodes all the necessary information about the coupling of the C atom with the rest of lattice. This spectral density was derived in Paper I using V_{at} as a "source" model, by effectively mapping it into an IO model. Here, we use the SD $J_C(\omega)$ that we obtained at the lowest temperature considered (T = 5 K), since this choice allows us to minimize the artifacts due to the anharmonicity of the system potential, as described at length in the related Paper I. Furthermore, the results presented below refer to collinear scattering calculations where the H atom was forced to lie on top of the binding C atom. The atomistic potential V_{at} which we started from[30] is based on an analytic fit to *first-principles* data[29] and on an empirical lattice model for graphene[37] and was briefly described in Paper I. Below we will also make use of such a model in *classical* calculations of the sticking probabilities in order to validate our system-bath model, analogously to the consistency checks reported in Paper I which concerned the equilibrium dynamics. The conceptual difference between the two is schematically represented in Fig. 1 where the environment around the carbon atom making the covalent bond with the incoming hydrogen changes from the graphene lattice in the atomistic description (left panel) to a set of independent oscillators (right panel).

Besides the environmental coupling, the PES describing the CH system is crucial for the success of the model. As mentioned above, the atomistic potential V_{at} relies on *first-principles* data fit to a convenient analytical expression which exploits the quasi-cylindrical symmetry of the interaction.[29] This *ab initio* C-H interaction potential, V_{CH}, was then coupled to the graphene force field via a Surface Oscillator (SO) model type coupling,[38] see Ref. 30 for details. The PES describes well known features of hydrogen chemisorption of graphene. The substrate experiences a strong reconstruction during the formation of the covalent bond, because of the change of hybridization of the binding carbon atom, from sp^2 to sp^3. The atom moves 0.426 Å out of the graphene sheet, thereby puckering the

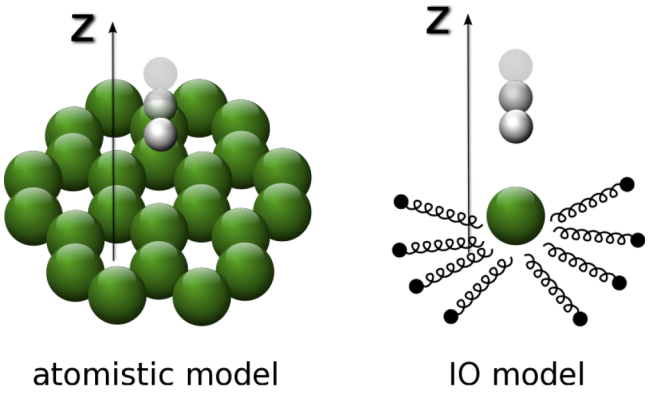

FIG. 1. Schematic representation of the dynamical models adopted in this work: the carbon cluster model, including a force field potential for the graphene phonon bath (left) and the IO model in which the bath is effectively described as a set of harmonic oscillators (right).

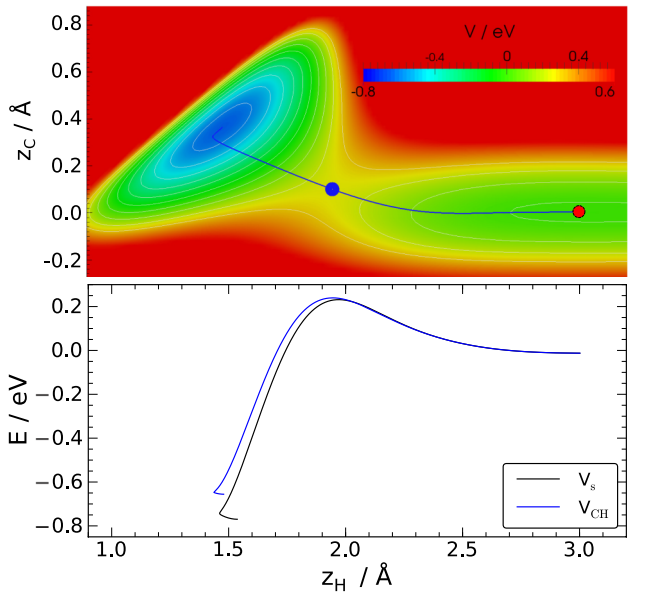

FIG. 2. Top: transition state (blue dot) and minimum energy path (blue line) connecting the physisorption minimum (red dot) to the chemisorption well (blue region), superimposed on a contour plot of the 2D collinear potential energy surface V_{CH} (contours are plotted every 100 meV). Bottom: the energy along the MEP as a function of the height of the H atom above the surface (z_H), for both the V_{CH} (blue) and the V_s (black) PES.

surface, to bind the hydrogen atom with a covalent bond which is 1.11 Å long and 0.767 eV more stable than the separated partners. The PES further describes a physisorption interaction which generates a shallow well when the projectile is far from the surface, at approximately 3.0 Å. The well is only ~9 meV deep, a value that is far from the accepted one of ~40 meV, which was obtained from the analysis of selective adsorption resonances in scattering experiments[39] and confirmed by accurate wavefunction-based calculations.[40] For the dynamics of the direct adsorption of a gas-phase hydrogen atom, where only collisions energies close to the barrier height of ~0.2 eV matter, the physisorption well is of minor importance. It has been though argued[35] that proper inclusion of the vdW dispersion forces affects not only the physisorption well but also the height and width of the sticking barrier, thereby enhancing both classical (above-barrier) and quantum (tunneling) sticking. This issue needs further investigation and, as mentioned in Paper I, work is already in progress to develop a new "system potential" that correctly accounts for the vdW interactions and accurately describes the physisorption well.

An overview of the CH interaction is given in Fig. 2 which depicts a cut of the PES through the 2D collinear configuration (upper panel). This figure clearly shows the deep chemisorption well, the entrance channel of the reaction, and the barrier between them. Also shown in the same figure is the minimum energy path (MEP) joining the weak physisorption well to the chemisorption region. To obtain such a MEP, the transition state (TS) was first located by using the Newton's optimization method and then the equation $\dot{\mathbf{x}} = -\hat{\mathbf{g}}(\mathbf{x})$ (where $\mathbf{x}$ is the set of mass-weighted coordinates and $\hat{\mathbf{g}}$ is the unit vector along the gradient of the PES with respect to these coordinates) was integrated with a Runge-Kutta 4th order algorithm. This MEP makes clear that a concerted motion of the two atoms is needed for adsorption to take place, at least at the low collision energies we are interested in. An outward motion of the carbon atom helps the sticking process, and an opposite movement strongly inhibits it. This suggests that lattice vibrations might play an important, *direct* role in determining the sticking probability, as confirmed by the results reported below.

The system potential of our IO model, V_s defined in Eq. (2), differs only slightly from the V_{CH} potential described above. The difference arises from a weak "renormalization" which occurs because of the coupling with the force field: when minimizing the atomistic potential V_{at} for fixed system coordinates $(\mathbf{x}_H, z_C)$, the puckering of the binding carbon causes a substantial curvature of the carbon cluster which increases slightly the hydrogen binding energy with respect to its flat surface value. This renormalization effect is tiny but it is important to take this into consideration when trying to compare dynamical results obtained from the lattice model with those obtained from the IO Hamiltonian of Eq. (1). In particular, the effect is already active at the transition state, where the carbon atom is only partially puckered, and gives rise to a small difference in the barrier energy as well. This is shown in Figure 2, bottom panel, which reports the energy along the MEP as a function of the z_H coordinate, for both the V_{CH} potential and the system potential, V_s. As can be seen from that figure, the barrier height in V_s is decreased with respect to that of V_{CH} (0.235 eV *vs.* 0.243 eV) and the binding energy increased (0.767 eV *vs.* 0.652 eV).

We notice at the outset that V_{CH} is likely more appropriate than V_s to describe H atom sticking — the lattice model V_{at} of the large but *finite* carbon cluster overemphasizes the role of surface relaxation — but if a strict comparison between the two models is desired, at least at a classical level, V_s defined above is most appropriate. Improvements in the description of the system potential are underway and will be the subject of a forthcoming publication. In this context, it is worth noticing that there is still no general consensus about the value of the barrier height. In V_{CH}, it is 0.243 eV, in agreement with several Generalized Gradient Approximation (GGA) DFT periodic calculations (all giving a barrier ~0.2 eV high), but recent calculations including van der Waals corrections have suggested that much lower values are more appropriate.[35]

Furthermore, accurate wavefunctions calculations on cluster models[41] show that GGA functionals overestimate (underestimate) the binding (barrier) energy, thereby opening the question of whether a higher level of theory on a cluster model is more appropriate than vdW-DFT on a periodic substrate. This uncertainty on the barrier height should always be kept in mind when comparing theoretical results to experiments.

III. METHODS

A. Molecular dynamics

In addition to the quantum dynamical calculations described below, we computed the sticking probability by means of classical and quasi-classical methods, since classical mechanics represents a stringent test for our system-bath modeling and further provides a simple mean to single out quantum effects in the results. Calculations were then performed with both the atomistic model V_{at} and the system-bath Hamiltonian of Eq. (1). Averages were computed over a set of 500-1000 trajectories, depending on the simulation, the smaller value being used for the system-bath Hamiltonian model in which V_s was computed by on-the-fly minimization of the cluster coordinates. In each trajectory, the hydrogen atom approaches the graphene surface at normal incidence, right above the binding carbon atom, to focus on the same collinear approach used for the quantum simulations. The surface (or the bath) was previously equilibrated at a given temperature via Langevin propagation with white noise. Then, in the case of the carbon cluster model, Langevin equilibration was maintained at the edges of the atomic cluster during the scattering dynamics, in order to mimic the conditions of an infinite surface. For the IO model, on the other hand, the bath of 300 oscillators which we used to sample the 0-900 cm^{-1} spectral density range had a recurrence time long enough (11 ps) to be effectively dissipative in the time interval used for the scattering dynamics. Quasi-classical trajectories involving zero-point motion of the bath were performed for the IO model only, replacing the equilibration step with the random sampling of the initial conditions on the phase-space orbit defined, for each harmonic oscillator, by its quantum zero-point energy.

Propagation was carried out for a total time of 500.0 fs, using a symplectic propagator for Langevin dynamics[42] that reduces to velocity-Verlet for $\gamma \to 0$. After this time, the sticking probability P_s was computed as the fraction of hydrogen atoms with $z_H < 2.646$ Å. Convergence of this probability was ensured by checking the trapped probability over time. Statistical error of the sticking probability ΔP_s was computed assuming a binomial distribution with Wilson score interval,

$$\Delta P_s \approx \frac{1}{1+\frac{1}{n}z^2}\left[\bar{P}_s + \frac{1}{2n}z^2 \pm z\sqrt{\frac{1}{n}\bar{P}_s\left(1-\bar{P}_s\right)+\frac{1}{4n^2}z^2}\right],$$

where n is the number of trajectories, $\bar{P}_s$ is the sticking probability estimated as average over the sample, and z is equal to 1.96 for a 95% confidence level. See Table I for a list of the main parameters used in the MD simulations.

TABLE I. Parameters of the MD simulations.

No. of trajectories	500/1000
Range of initial H incident energy (eV)	0.18–0.6
Initial height of the H atom (Å)	6.0
Surface equilibration Δt (fs)	0.02
Surface equilibration γ_{eq}^{-1} (fs)	50.0
Surface equilibration time (fs)	200.0
Surface temperature (K)	50.0, 300.0
Propagation Δt (fs)	0.01
Relax at the edges γ^{-1} (fs)	∞, 1000, 100
Propagation time (fs)	500

B. Quantum dynamics

Quantum simulations were performed with the multi-configuration time-dependent Hartree (MCTDH) method (Heidelberg MCTDH package[43–46]). Only the IO Hamiltonian was considered since, as already stressed in Paper I, quantum dynamics is not feasible with the carbon cluster model. A bath of 25 harmonic oscillators was sufficient for sampling the low energy range of the spectral density, between 0 and 900 cm^{-1}. Indeed, this discretization of the bath gives rise to a recurrence time of about 927 fs, which is long enough to obtain converged results.

The initial wavefunction along the z_H degree of freedom was chosen to be a Gaussian wavepacket, using six different values of the average momentum to cover a large collision energy range. For the remaining degrees of freedom — the C atom and the harmonic bath coupled to it — the ground state of the Hamiltonian appropriate when $z_H \to \infty$ was obtained by imaginary-time propagation. After this initial relaxation step, the wavefunction was then propagated in real time with the full Hamiltonian of Eq. (1). The reflected fraction of the wavepacket was absorbed by a cubic optical potential and its probability was flux-analyzed along z_H and time-energy mapped to give energy-resolved probabilities. The outcome of the above six wavepacket calculations was then carefully checked to overlap at common energies and joined to give a unique smooth curve in the 0.1-0.9 eV collision energy range.

For the primitive representation of the wavefunction, we used a uniform grid for z_H and z_C (160 points for z_H and 48 for z_C) and a Hermite basis set with appropriate mass and harmonic frequency for the other bath degrees of freedom (6 for each of the q_i's). The converged single particle basis employed is composed of a single mode for the system (with 20 single particle functions) and 5 modes of five oscillators each for the bath (8 single particle functions per each mode). See Table II for a list of all the main parameters of the quantum dynamics simulations.

IV. RESULTS AND DISCUSSION

Before discussing the quantum dynamical results, it is instructive to first focus on some classical aspects of the sticking process. Figure 3 shows the results of classical molecular dynamics simulations obtained with the atomistic potential

TABLE II. Parameters of the quantum dynamical simulations.

Average momentum (a_0^{-1})	3	4.5	5	7	8.5	10
z_H wavepacket width (a_0)	1.1	0.8	0.8	0.45	0.45	0.45
Final propagation time (fs)	1200	900	800	600	600	600
z_H grid minimum (a_0)	1.5	1.5	1.5	1.0	1.0	1.0
z_H grid maximum (a_0)	30.0	24.0	24.0	18.0	16.0	15.0
z_C grid minimum (a_0)	−0.8	−0.8	−0.8	−0.8	−0.8	−0.8
z_C grid maximum (a_0)	1.8	1.8	1.8	1.8	1.8	1.8
Absorption potential strength (E_h)	1.4×10^{-6}	1.4×10^{-5}	1.62×10^{-5}	8.97×10^{-5}	4.174×10^{-4}	1.2×10^{-3}
z_H of the flux line (a_0)	14	14	14	11	11	11

appropriate for the cluster model described in Paper I, for two different surface temperatures, T = 50 and 300 K. At low temperature, the sticking probability is negligibly small below the (static) barrier energy and reaches a saturation value P_s = 1.0 at higher energies in a relatively narrow energy range.

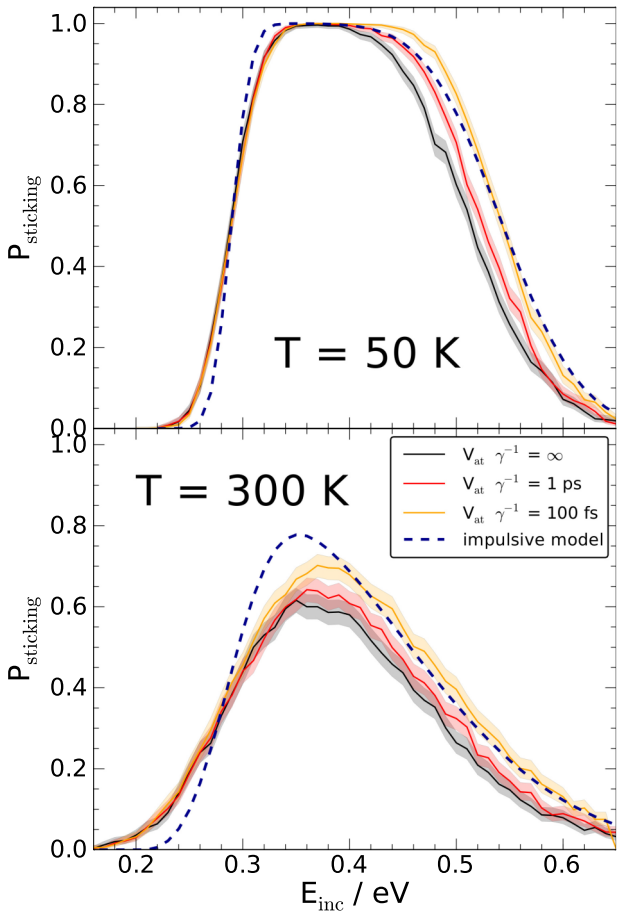

FIG. 3. Classical H atom sticking probability computed with the atomistic potential V_{at} at two different surface temperatures, T = 50 K (top panel) and T = 300 K (bottom panel), as a function of the collision energy. Results are computed with Langevin atoms at the cluster edges using different relaxation times (black: $\gamma^{-1} = \infty$, red: γ^{-1} = 1 ps, and orange: γ^{-1} = 100 fs), and statistical errors are given as shaded areas around estimated values. Dashed lines are fitting of the MD results with γ^{-1} = 100 fs to the impulsive model expression of Eq. (3) (see text for details).

In this transition range, sticking is mainly determined by the probability that the incoming hydrogen overcomes the barrier since any H atom that reaches the interaction region is able to dissipate the small amount of energy in excess to the barrier and gets trapped in the chemisorbed well. As a consequence, no significant difference is found in P_s at these energies when employing different values of the relaxation time γ^{-1} for the Langevin atoms at the cluster edges (see Fig. 3).

At energies above the saturation value, the sticking probability decreases, eventually after a quasi-*plateau* region that is evident in the low temperature simulations (Fig. 3, top panel). In this case, projectile atoms have enough energy to reach the chemisorption well, but sticking only occurs if energy relaxation is efficient enough to prevent the projectile to re-cross the barrier and return to the gas-phase. As a consequence, in this collision energy regime, relaxation at the edges of the cluster model does play some role, and the faster the relaxation the larger the sticking probability. Reasonable values of γ^{-1} are in the range 100–1000 fs, but results obtained with no dissipation at the cluster edges ($\gamma^{-1} = \infty$) represent useful lower bound for the sticking probabilities.[47]

The arguments given above find substantial quantitative support from the analysis of a simple one-dimensional model of the scattering process. In this model, the energy available to the projectile for overcoming the barrier in the relative CH coordinate is the kinetic energy of H *relative* to C, and this is determined by both the projectile energy E and the thermal agitation of the surface atom. Assuming that the projectile atom travels towards the C atom (leftward), for each given collision energy E, the barrier-crossing condition requires that the carbon atom speed v_C exceeds a threshold value v_{th},

$$v_C \geq v_{th}(E) \equiv -|v_H| + v_b,$$

where $v_H^2 = 2E/m_H$, $v_b^2 = (1+\chi)2E_b/m_H$, $\chi = m_H/m_C$ is the projectile-target mass ratio and E_b the barrier height. Once the atom has crossed the barrier, it is accelerated by the attractive interaction with the surface atom and energy transfer takes place, depending on v_C, hence on the surface temperature T. It is straightforward to estimate the condition under which the transferred energy is enough for trapping to occur by looking at the impulsive limit, which is appropriate at the high collision energies where energy dissipation dominates. As is shown in

Appendix A, trapping only occurs if v_C lies in the interval

$$I_i(E) = [v_-, v_+], \quad v_\pm(E) = -\frac{1-\chi}{2}|\tilde{v}_H| \pm \frac{1+\chi}{2}v_0,$$

where

$$\tilde{v}_H^2 = \frac{2(E+D)}{m_H} \quad v_0^2 = \frac{2(E_b+D)}{m_H}$$

and D is an "effective" depth for the interaction well. Hence, if this hard-collision limit kept down to low energies, the sticking probability would be solely determined by the two conditions above and could be simply obtained by integrating the distribution of the carbon atom velocities over an energy dependent domain $\Sigma(E) = I_i(E) \bigcap [v_{th}(E), +\infty)$, namely, as

$$P_s(E) = \int_{\Sigma(E)} g(v)dv, \tag{3}$$

where

$$g(v) = \left(\frac{m_C}{2\pi k_B T}\right)^{1/2} e^{-\frac{m_C v^2}{2k_B T}}$$

is the Maxwell-Boltzmann distribution appropriate for this classical bath case. The model is quite crude but suffices to capture the essential physics of this sticking process, both at low and at high energies, with the help of two system parameters only, namely, the barrier height E_b and the effective well depth D. Fitting the $T = 50$ K MD results to Eq. (3) gave surprisingly good results (see dashed lines in Fig. 3, top panel) with $E_b = 0.267$ eV and $D = 0.424$ eV, which were further confirmed at higher temperature (Fig. 3, bottom panel), where we used the same E_b and optimized the well depth only ($D = 0.207$ eV). Figure 3 clearly shows that, despite obvious problems at low energies where collisions cannot be impulsive, the model correctly describes the general behavior of the sticking curves, e.g., the presence of a *plateau* at low temperatures and the reduction of the saturation value when increasing the temperature. Note only that in light of its marked temperature dependence, the well depth D is better regarded as an effective dynamical parameter rather than a true feature of the interaction potential; in the model, it is the only parameter controlling the energy transfer, thereby replacing both the CH interaction and the energy dissipation to the lattice.

Next we consider the IO model in the classical setting. Figure 4 shows the sticking probability obtained from the Hamiltonian of Eq. (1). Two different system potentials were considered — V_s as defined above and V_{CH} — in order to investigate the influence of the system potential on the dynamical outcome, and results were compared with those obtained with the atomistic model reported in Fig. 3. The agreement is very good, particularly in the transition regime and for the potential V_s, thereby justifying our choice of the system potential. Above saturation, the IO models predict a lower sticking probability than the original lattice model with no relaxation at the cluster edges, irrespective of the system potential, though the discrepancy is reduced when increasing the surface temperature (Fig. 4, bottom panel). This is a clear limitation of the IO modeling, which fails to provide enough dissipation for highly energetic H atom projectiles impinging on the surface. Although it could likely be amended by extending the model to include state-dependent friction — i.e., by replacing the coupling linear in z_C with a function $f(z_C)$ which reduces to z_C close to equilibrium but increases for larger displacements of the carbon atom — we are not interested in such an energy regime, since it is essentially classical and can be efficiently handled with molecular dynamics (it is actually well described by the impulsive model introduced above). Importantly, the IO model quantitatively reproduces the results of the full atomistic potential below saturation, and the magnitude of the saturation value, thereby providing a good degree of confidence that the quantum results described below are truly representative of the original atomistic model.

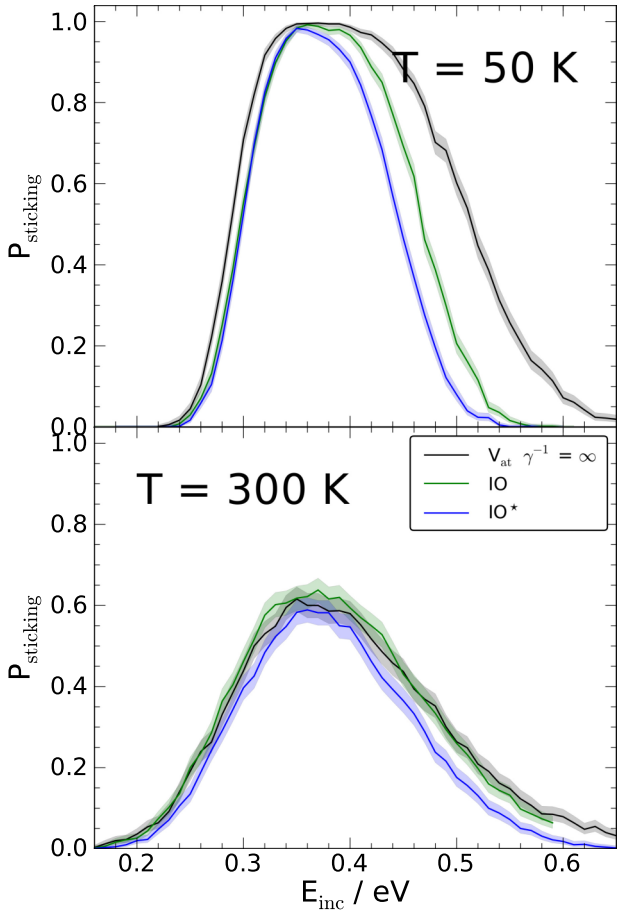

FIG. 4. Classical H atom sticking probability at two different bath temperatures, $T = 50$ K (top panel) and $T = 300$ K (bottom panel), as a function of the collision energy. Two different IO models are used, differing only in the choice of the system potential, green for V_s and blue for V_{CH}. Also shown are the results obtained with the atomistic model reported in Fig. 3 (black curve), with no relaxation at the edges ($\gamma^{-1} = \infty$). Statistical errors are given as in Fig. 3.

Finally, we consider the results of the quantum scattering calculations that were performed with the IO model, using the collinear 2D system Hamiltonian and $F = 25$ bath oscillators. As mentioned in Section III, only the low frequency range of the spectral density $J_C(\omega)$ (i.e., $\omega \lesssim 900$ cm^{-1}) was sampled, but test quantum calculations on larger models and the classical results described above suggest that this is indeed quite a good approximation. Several wavepackets were propagated to cover the relevant energy range, and reflection was flux-analysed (and time-energy mapped) for times long enough to obtain converged results but small enough to prevent the effects of the finite-bath recurrences. An overview of a typical

quantum dynamics simulation is given in Fig. 5, left panel, where the probability density along z_H is plotted as a function of time. The figure clearly shows that when the scattering wavepacket gets near to the surface, only a small fraction of it is directly reflected (at the considered energy) while the largest fraction overcomes the barrier and reaches the adsorption well. A residual fraction is expelled in some tens of fs and forms an inelastically scattered fraction, and most of the wavepacket remains trapped in the adsorption well and relaxes. Figure 5, right panel, gives the corresponding time-evolution of the bath excitation, as given by the average occupation number of the oscillators (average number of phonons). Excitation first involves the high frequency modes only but in a rather narrow time interval (some tens of fs) spreads over the whole frequency range, exhibiting a pattern that closely parallels the maxima of the spectral density. This is due to the strong coupling between the bath and the surface stretching mode, whose relaxation was discussed in Paper I.

On combining the energy resolved results of several wavepacket simulations, the quantum mechanical sticking probability curve illustrated in Fig. 6 was obtained. Also depicted, for comparison, are the classical results obtained at the lowest temperature considered, $T = 50$ K. The two sets of results differ both in the low collision energy regime where quantum effects (tunneling) are expected and in the high energy regime, where a classical mechanical description holds for the projectile dynamics. This is clearly due to the quantum nature of the low temperature surface that in this $T = 0$ K limit shows pronounced zero-point energy effects on the projectile dynamics. This can be checked with the aid of the classical impulsive model introduced above which, as shown in Fig. 3,

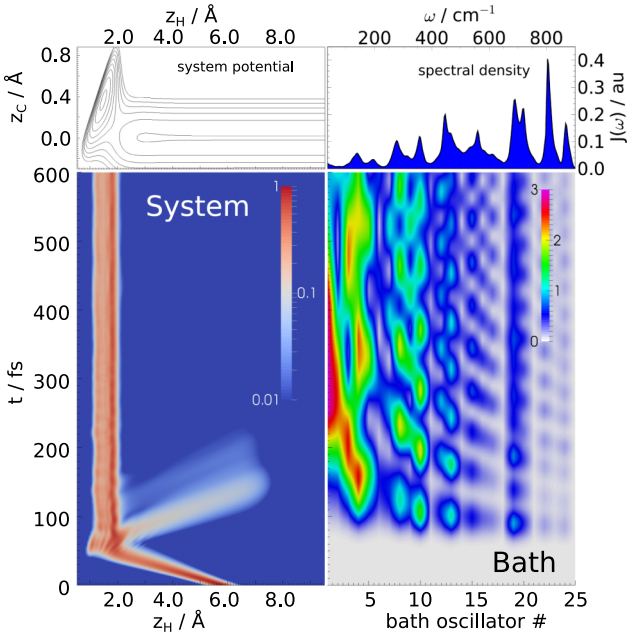

FIG. 5. Time evolution of the reduced density along z_H (left bottom panel) and of the average excitation number of the bath oscillators (right bottom panel) in a typical quantum simulation. The average initial momentum was 7 a.u., corresponding to a nominal collision energy of 0.36 eV. The top panel on the left shows a contour plot of the system potential aligned along z_H, and the top panel on the right gives the spectral density $J_C(\omega)$ as a function of frequency, in correspondence with the bath oscillator number.

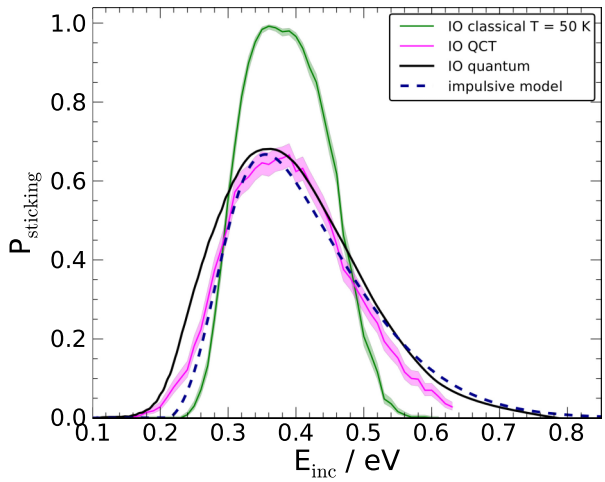

FIG. 6. Sticking probability as a function of the collision as obtained from the quantum dynamical calculations described in the main text (black curve). Also shown for comparison the classical (green) and the quasi-classical (magenta) results obtained at $T = 0$ K with the same IO model, and a fit to the impulsive model expression of Eq. (3) using the $T = 0$ K quantum distribution of the carbon atom velocities (dashed lines). Shaded areas around classical and quasi-classical curves represent statistical uncertainties, similarly to Fig. 3.

provides quite a good representation of the system dynamics. Adopting a mixed classical-quantum description where the low temperature bath is treated quantally, the sticking probability follows again from Eq. (3) with $g(v)$ replaced by the appropriate velocity distribution of the carbon atom quantum oscillator, *coupled* to the rest of the lattice. As is shown in Appendix B, the required function $g_q(v)$ is given by

$$g_q(v) = \sqrt{\frac{m_c}{\pi\hbar\Omega_T}}\, e^{-\frac{m_c v^2}{\hbar\Omega_T}},$$

where the temperature-dependent effective frequency Ω_T accounts for the coupling to the bath and can be given in terms of the spectral density $J_H(\omega)$ of any probe species (e.g., the H atom considered in this work) bilinearly coupled to the bath by means of the carbon atom only,[48]

$$\Omega_T = \frac{\int_0^{+\infty} d\omega J_H(\omega)\omega^2 \coth\left(\frac{\hbar\omega}{2k_B T}\right)}{\int_0^{+\infty} d\omega J_H(\omega)\omega}.$$

This effective frequency takes the lowest value in the $T = 0$ K limit,

$$\Omega_0 = \frac{\int_0^{+\infty} d\omega J_H(\omega)\omega^2}{\int_0^{+\infty} d\omega J_H(\omega)\omega}$$

($\Omega_0 = 599.3$ cm^{-1} in the case considered here) and increases linearly with T at high temperatures,

$$\Omega_T \approx \frac{2k_B T}{\hbar}$$

provided the thermal energy is much larger than the zero point energy at the Debye cut-off frequency of the bath, $k_B T \gg \hbar\omega_D/2$. In this limit, of course, $g_q(v)$ reduces to the classical Maxwell-Boltzmann distribution, irrespective of the coupling to the rest of the lattice. Fitting the quantum results to Eq. (3) using $g_q(v)$ for $T = 0$ K (the barrier height being fixed to the value obtained from the classical simulations) gives a

satisfactory agreement (Fig. 6, dashed line) over the whole energy range with $D = 0.183$ eV despite the limitations of the model at low energies, thereby confirming the primary role of the zero point motion of the lattice. We further performed zero-temperature quasi-classical simulation of the dynamics to overcome the limits of the impulsive model at low energies and single out the genuine quantum effects in the system dynamics. The results of these simulations are reported in Fig. 6 and show a rather good agreement with the quantum results, apart from the threshold region where tunneling through the barrier occurs. A close-up of this energy region is given in Fig. 7, where the same results above are plotted on a logarithmic scale. This figure shows that the effect of the tunneling dynamics is moderate (less than one order of magnitude), at least for energies not too small compared to the barrier height. This should be contrasted with the effect of the lattice quantum fluctuations which, for energies close to the barrier height, increase the probability by about two orders of magnitudes. It remains to be established to which extent this conclusion is modified when refining the system potential to account for the vdW interactions, and whether the conclusions drawn by Davidson *et al.*[35] for the physisorbed-to-chemisorbed transition rate can be extended to the direct dynamics considered here.

The quantum collinear sticking probability computed here is much larger than the results recently obtained by Karlický *et al.*,[34] which show a saturation value of the sticking probability of about 20% for a similar collinear model. The authors of Ref. 34 used a fully quantum methodology with an explicit description of the bath and computed the relevant couplings from *first principles*. However, in order to keep the problem numerically tractable, they had to enforce a single-phonon approximation. Figure 5, on the other hand, clearly shows that a large amount of energy is transferred to the bath, i.e., multiphonon relaxation is operative, especially for low frequency oscillators. Given the primary role that relaxation plays in this process, and its influence on the shape of the sticking curve and on the saturation value, the underestimation of the sticking probability in Ref. 34 appears to be mainly due to the failure of the one-phonon (Tamm-Dancoff) approximation.

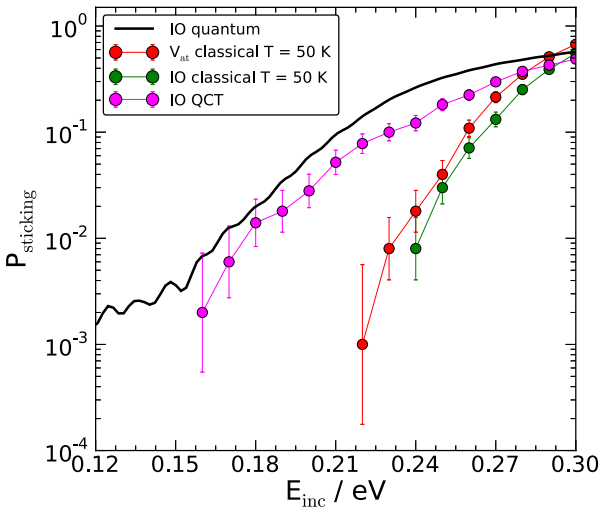

FIG. 7. Close-up of the sticking probability curves (on a logarithmic scale) shown in Fig. 6, for energies close to the barrier height (~0.24 eV). Color coding is as in Fig. 6 and vertical bars represent statistical uncertainties.

Unfortunately, a direct comparison between our results and experimental works seems to be inappropriate at present, for two main reasons. First, the moderate-to-high coverage regime in which experiments have been performed involves a substantial formation of hydrogen dimers and clusters, whose rate is hard to disentangle from the single atom adsorption considered in this work. Secondary adsorption can be non-activated or weakly activated in the neighborhoods of a previously adsorbed H atom, depending on the specific lattice position,[27] and dominates the hydrogen uptake rate unless special care is used to limit the surface coverage. Second, our theoretical modeling still needs important refinements concerning both the interaction potential and the dynamics. As mentioned in the Introduction, the precise value of the height of the adsorption barrier is yet unknown and this currently prevents any reliable estimate of the sticking probability at the low collision energies that are relevant for the chemistry of the ISM. Furthermore, the present dynamical simulations are limited by the reduced dimensionality of the collisions investigated, and the role of non-collinear approaches of the H atom to the binding carbon atom is yet to be assessed in the quantum setting (for the classical case see, e.g., Ref. 29). Work is currently in progress to address both issues.

V. CONCLUSIONS

The scattering dynamics of a H atom on a $T = 0$ K graphene surface was investigated using a fully quantum method, with a focus on the collinear approach. On comparing the results with classical and quasi-classical calculations, we validated the independent oscillator model developed in Paper I, and elucidated the essential physics governing the sticking dynamics. Two main factors governing the dynamics were singled out, i.e., barrier crossing and energy transfer, and it was shown that quantum fluctuations play a primary role in the process. Furthermore, a simple impulsive model capturing all these physical effects was developed. The model describes the collision of a *classical* projectile with a *quantum* surface and reproduces the quantum results with remarkable agreement for all but the lowest energies, where the collision is no longer impulsive and tunneling of the projectile through the adsorption barrier cannot be neglected.

ACKNOWLEDGMENTS

This work has been supported by Regione Lombardia and the CINECA High Performance Computing Center through a LISA Initiative (2014) grant. B. Jackson gratefully acknowledges support from the Division of Chemical Sciences, Office of Basic Energy Science, Office of Energy Research, U.S. Department of Energy, under Grant No. DE-FG02-87ER13744.

APPENDIX A: IMPULSIVE MODEL

We derive in this appendix the conditions that the carbon atom velocity has to fulfill for trapping to occur in the

impulsive limit. In this limit, the hydrogen atom traveling with velocity $\tilde{v}_H$ undergoes a hard collision with a carbon atom that is essentially free and moves at a speed v_C. Denoting V the center of mass speed and $v = \tilde{v}_H - v_C$ the relative velocity of the colliding pair, the effect of the collision is simply to revert the relative velocity, i.e., in the laboratory frame, $\tilde{v}_H = V + \frac{\mu}{m_H} v \to v'_H = V - \frac{\mu}{m_H} v$, where μ is the reduced mass. Hence, the energy transferred to the carbon atom, $\delta\epsilon = E - E'$, is given by

$$\delta\epsilon = 2\mu V v = \frac{4\chi(E + D - \frac{1}{2}m_C v_C^2) + 2\chi(1-\chi)m_C \tilde{v}_H v_C}{(1+\chi)^2},$$

where E, E' are the pre- and post-collisional energy of the hydrogen atom, $\chi = m_H/m_C$ is the projectile-target mass ratio, and D is the well depth accelerating the projectile before bouncing (here and in the following, energy is measured with respect to the free partners, $\tilde{v}_H^2 = 2(E+D)/m_H$ and $v_H^2 = 2E/m_H$). Soon after collision has occurred, the carbon atom rapidly dissipates its energy to the lattice and comes to rest. Hence, the post-collision energy $E' = E - \delta\epsilon$ is also the energy in the relative motion which is relevant for trapping. Specifically, in the presence of a barrier of height E_b, the trapping condition reads as

$$E' = E - \delta\epsilon < E_b$$

and leads to

$$v_C^2 - (1-\chi)v_C\tilde{v}_H + \frac{1}{2m_H}\left[(1-\chi)^2 E - (1+\chi)^2 E_b - 4\chi D\right] < 0.$$

This equation is satisfied provided $v_- < v_C < v_+$, where

$$v_\pm = v_C^{max} \pm \frac{1+\chi}{2} v_0,$$

with

$$v_C^{max} = -\frac{1-\chi}{2}|\tilde{v}_H| \quad v_0 = \sqrt{\frac{2(E_b+D)}{m_H}}$$

and the projectile has been assumed to move leftward (note that $v_- > -|\tilde{v}_H|$ holds, thereby guaranteeing that collision occurs). It follows that the carbon atom velocities need to be picked up from an interval $(1+\chi)v_0$ wide which is centered around the energy-dependent value v_C^{max}. The latter is the carbon atom velocity that maximizes the energy transfer $\delta\epsilon$ and stops the projectile since the post-collisional speed

$$v'_H = V - \frac{\mu}{m_H} v \equiv \frac{1-\chi}{1+\chi}|\tilde{v}_H| + \frac{2}{1+\chi} v_C$$

vanishes for $v_C = v_C^{max}$ above. Notice that for $v_C < v_C^{max}$ the projectile undergoes *multiple* collision events and additional trapping might occur beyond the "direct trapping" window $v_C \in [v_-, v_+]$: when $v_C < v_-$ (but such that $v_C > -|\tilde{v}_H|$, for the first collision to occur), projectiles that are not trapped at the first bounce may dissipate the excess energy after a number of collisions. In the main text, we did *not* consider this possibility, since the barrier crossing condition $v_C > -|v_H| + v_b$ (where $v_b^2 = (1+\chi)2E_b/m_H$) provides typically a more stringent lower bound on v_C.

APPENDIX B: VELOCITY DISTRIBUTION OF A QUANTUM HARMONIC OSCILLATOR COUPLED TO A HEAT BATH

We derive in this appendix the equilibrium velocity distribution of a harmonic oscillator coupled bilinearly to a bath, considering first the case of a discretized bath. Let x_0, p_0 be the position and the momentum operators of the oscillator and m its mass. The momentum distribution $\rho(p)$ of interest can be expressed as the inverse Fourier transform of the following characteristic function:

$$\hat{\rho}(\xi) = \langle e^{i\xi p_0} \rangle,$$

where $\langle \ldots \rangle$ denotes the thermal equilibrium average. The momentum operator p_0 is given as superposition of normal mode momenta P_k of the overall system

$$p_0 = \sum_k U_{0k} P_k$$

with some yet unspecified coefficients. The equilibrium state of the system is a product state in the normal mode representation

$$\hat{\rho}(\xi) = \prod_k \hat{\phi}_k(U_{0k}\xi),$$

where $\hat{\phi}_k$ is the momentum characteristic function of the kth normal oscillator,

$$\hat{\phi}_k(\xi) \equiv \exp\left(-\frac{m\hbar\Omega_k}{4}\coth\left(\frac{\hbar\Omega_k}{2k_BT}\right)\xi^2\right).$$

Here, Ω_k is its eigenfrequency and m is a convenient choice of the mass. Accordingly, $\hat{\rho}(\xi) = \exp\left(-\frac{m\hbar\Omega_T}{4}\xi^2\right)$, where the effective (temperature-dependent) frequency Ω_T is given as an average over the eigenmodes

$$\Omega_T = \sum_k |U_{0k}|^2 \Omega_k \coth\left(\frac{\hbar\Omega_k}{2k_BT}\right)$$

and the required momentum distribution follows as

$$\rho(p) = \frac{1}{\sqrt{\pi m\hbar\Omega_T}} e^{-\frac{p^2}{m\hbar\Omega_T}}.$$

It then remains to find a suitable expression for U_{0k}, which is a problem in classical mechanics. Suppose we are given a set of N coupled oscillators of equal mass m, for simplicity. Let $\mathbf{x}^t = (x_0, x_1, \ldots, x_{N-1})$ be their coordinates, x_0 being the degree of freedom we are interested in. Then, $U_{0k} = (\mathbf{U})_{0k}$ for $k = 1, \ldots, N$, where the (orthogonal) matrix $\mathbf{U}$ is just the matrix of the eigenvectors of the dynamical matrix $\mathbf{V}$ entering the classical Lagrangian

$$L = \frac{m}{2}\dot{\mathbf{x}}^t\dot{\mathbf{x}} - \frac{m}{2}\mathbf{x}^t\mathbf{V}\mathbf{x}.$$

We only need the first row, and we are free to choose the set of original oscillators to start with, depending of the kind of information that is available about the coupling. If this information is subsumed in a spectral density $J_C(\omega)$, the "bath" $x_1, x_2, \ldots, x_{N-1}$ is in normal form and, for $k, l = 1, \ldots, N-1$,

$$\mathbf{V}_{00} = \omega_0^2, \ \mathbf{V}_{0k} = \mathbf{V}_{k0} = -\frac{c_k}{m}, \ \mathbf{V}_{kl} = \delta_{kl}\omega_k^2,$$

where, for instance, the bath frequencies are evenly spaced $\omega_k = k\Delta\omega$ and $c_k = \sqrt{2\,m\,\omega_k\,\Delta\omega\,J_C(\omega_k)/\pi}$. Due to the simple

structure of $\mathbf{V}$, the problem is readily solved to give

$$|U_{0k}|^2 = \frac{1}{1 + \sum_{l=1}^{N-1} \frac{c_l^2}{(\omega_l^2 - \Omega_k^2)^2}}$$

provided the eigenfrequencies Ω_k *are known*. Ω_k's satisfy the simple-looking equation in the unknown Ω,

$$\Omega^2 - \omega_0^2 + \sum_{l=1}^{N-1} \frac{c_l^2}{\Omega^2 - \omega_l^2} = 0$$

which though has no general, known solution.

Fortunately, we are interested in the continuum limit where no such need arises. Here, we consider this limit from scratch, introducing the functions $x(\omega), \dot{x}(\omega)$ in place of $x_k, \dot{x}_k$, in conjunction with $x_0, \dot{x}_0$ for the mode we are interested in, in such a way that $(x_0, x(\omega))$ represents a generic configuration of the system. Such functions are square integrable, on account of the finiteness of both the kinetic and the potential energies; hence, the problem can be formulated in a standard Hilbert space, V being an operator in such space which replaces the previous $\mathbf{V}$. For convenience, we use Dirac-like notation and abstract state vectors $|0\rangle$ and $|\omega\rangle$ for the system and the bath, with the orthogonality conditions

$$\langle 0|0\rangle = 1 \; \langle 0|\omega\rangle = \langle \omega|0\rangle = 0$$

and

$$\langle \omega|\omega'\rangle = \delta(\omega - \omega').$$

With this notation, $|0\rangle$ and $|\omega\rangle$ are unit displacement vectors of the system and of the ω-bath oscillator, respectively — they correspond to the choices $(x_0, x(\omega')) \equiv (1, 0)$ and $(x_0, x(\omega')) \equiv (0, \delta(\omega - \omega'))$ — and a generic configuration of the overall system can be written as

$$|\psi\rangle = x_0|0\rangle + \int d\omega x(\omega)|\omega\rangle$$

(and similarly for its velocity vector $|\dot{\psi}\rangle$) and the Lagrangian above takes the simple form

$$L[\psi, \dot{\psi}] = \frac{m}{2}\langle \dot{\psi}|\dot{\psi}\rangle - \frac{m}{2}\langle \psi|V|\psi\rangle,$$

where V is a self-adjoint operator

$$V = \omega_0^2|0\rangle\langle 0| - |\zeta\rangle\langle 0| - |0\rangle\langle \zeta| + \int d\omega \omega^2 |\omega\rangle\langle \omega|,$$

with

$$|\zeta\rangle = \frac{1}{m}\int d\omega c(\omega)|\omega\rangle.$$

Here, $c(\omega)$ is related to the spectral density, $c(\omega)^2 = 2m\omega J_C(\omega)$, in agreement with the uniform quadrature rule of the scalar product, e.g., $x_k = \sqrt{\Delta\omega}x(\omega_k)$. Having established this setting, the quantity of interest is easily related to the Green's operator $G(z) = (z - V)^{-1}$, and its matrix element $G_{00} = \langle 0|G|0\rangle$,

$$|U_{0k}|^2 \to -\frac{1}{\pi}\lim_{\epsilon \to 0^+} G_{00}(y + i\epsilon) \;\; (y \in \mathbb{R}^+)$$

as it follows from the spectral representation of G in terms of the eigenvectors $|y\rangle$, i.e., the normal modes, where $y = \Omega^2$ are the squared eigenfrequencies. In turn, finding G_{00} becomes a standard problem which can be easily solved using projector-operator techniques (V above is indeed isomorphic to the celebrated [non-interacting] Anderson Hamiltonian describing an impurity level in a host material[49]). The result reads as

$$G_{00}(z) = \frac{1}{z - \omega_0^2 - \frac{2}{\pi}\int_0^\infty \frac{J_C(\omega)\omega}{z - \omega^2} d\omega}.$$

At this point, it is convenient to introduce the function $W(z) = -G_{00}(z^2)$ which has similar limit as G_{00} above, namely, for $z = \omega + i\epsilon$ ($\omega > 0$),

$$|\mathcal{U}_{0,\omega^2}|^2 = \frac{1}{\pi}\lim_{\epsilon \to 0^+} W(\omega + i\epsilon),$$

where $\mathcal{U}_{i,k}$ is the continuum version of the normal mode transformation U_{ik}. The function

$$W(z) \equiv \frac{1}{\omega_0^2 - z^2 - \frac{1}{\pi}\int_{-\infty}^{+\infty} \frac{J_C(\omega)}{\omega - z} d\omega}$$

is essentially the propagator introduced in Ref. 50 describing the coupling to an oscillator of frequency ω_0, which in turn is coupled to a bath. Using the results of Ref. 50, the required limit becomes

$$\Im W^+(\omega) = \frac{\pi J_H(\omega)}{2\int_0^\infty J_H(\omega)\omega d\omega},$$

where $J_H(\omega)$ is the spectral density felt by an arbitrary "probe" coupled bilinearly to x_0. Finally, the sum over eigenmodes transforms to

$$\sum_k |U_{0k}|^2(\ldots) \to \int d(\omega^2)\frac{\Im W^+(\omega)}{\pi}(\ldots)$$

and we obtain the desired expression for Ω_T as

$$\Omega_T = \frac{\int_0^\infty \omega^2 \coth\left(\frac{\hbar\omega}{2k_BT}\right) J_H(\omega)d\omega}{\int_0^\infty \omega J_H(\omega)d\omega}.$$

This completes our derivation for the momentum distribution function $\rho(p)$. $g_q(v)$ then takes the form

$$g_q(v) = \sqrt{\frac{m_c}{\pi\hbar\Omega_T}} e^{-\frac{m_c v^2}{\hbar\Omega_T}}.$$

Note that in absence of coupling (i.e., $J_C(\omega) \equiv 0$), $J_H(\omega)$ reduces to a δ–peak centered around ω_0 and Ω_T above only depends on the bare frequency of the oscillator.

[1] L. Jeloaica and V. Sidis, Chem. Phys. Lett. **300**, 157 (1999).
[2] X. Sha and B. Jackson, Surf. Sci. **496**, 318 (2002).
[3] T. Zecho, A. Güttler, X. Sha, B. Jackson, and J. Küppers, J. Chem. Phys. **117**, 8486 (2002).
[4] R. J. Gould and E. E. Salpeter, Astrophys. J. **138**, 393 (1963).
[5] D. Hollenbach and E. E. Salpeter, Astrophys. J. **163**, 155 (1971).
[6] S. T. Bromley, T. P. M. Goumans, E. Herbst, A. P. Jones, and B. Slater, Phys. Chem. Chem. Phys. **16**, 18623 (2014).
[7] D. C. Elias, R. R. Nair, T. M. G. Mohiuddin, S. V. Morozov, P. Blake, M. P. Halsall, A. C. Ferrari, D. W. Boukhvalov, M. I. Katsnelson, A. K. Geim, and K. S. Novoselov, Science **323**, 610 (2009).
[8] A. Bostwick, J. L. McChesney, K. V. Emtsev, T. Seyller, K. Horn, S. D. Kevan, and E. Rotenberg, Phys. Rev. Lett. **103**, 056404 (2009).
[9] R. Balog, B. Jorgensen, L. Nilsson, M. Andersen, E. Rienks, M. Bianchi, M. Fanetti, E. Laegsgaard, A. Baraldi, S. Lizzit, Z. Sljivancanin, F. Besenbacher, B. Hammer, T. G. Pedersen, P. Hofmann, and L. Hornekaer, Nat. Mater. **9**, 315 (2010).
[10] D. Haberer, D. V. Vyalikh, S. Taioli, B. Dora, M. Farjam, J. Fink, D. Marchenko, T. Pichler, K. Ziegler, S. Simonucci, M. S. Dresselhaus, M. Knupfer, B. Büchner, and A. Grüneis, Nano Lett. **10**, 3360 (2010).

[11]K. Tada, J. Haruyama, H. X. Yang, M. Chshiev, T. Matsui, and H. Fukuyama, Phys. Rev. Lett. **107**, 217203 (2011).
[12]T. Zecho, A. Güttler, and J. Küppers, Carbon **42**, 609 (2004).
[13]A. Güttler, T. Zecho, and J. Küppers, Chem. Phys. Lett. **395**, 171 (2004).
[14]A. Andree, M. L. Lay, T. Zecho, and J. Küppers, Chem. Phys. Lett. **425**, 99 (2006).
[15]L. Hornekær, Ž. Šljivančanin, W. Xu, R. Otero, E. Rauls, I. Stensgaard, E. Lægsgaard, B. Hammer, and F. Besenbacher, Phys. Rev. Lett. **96**, 156104 (2006).
[16]L. Hornekær, E. Rauls, W. Xu, Ž. Šljivančanin, R. Otero, I. Stensgaard, E. Lægsgaard, B. Hammer, and F. Besenbacher, Phys. Rev. Lett. **97**, 186102 (2006).
[17]S. Baouche, G. Gamborg, V. V. Petrunin, A. C. Luntz, A. Baurichter, and L. Hornekær, J. Chem. Phys. **125**, 084712 (2006).
[18]R. Balog, B. Jørgensen, J. Wells, E. Lægsgaard, P. Hofmann, F. Besenbacher, and L. Hornekær, J. Am. Chem. Soc. **131**, 8744 (2009).
[19]E. Aréou, G. Cartry, J.-M. Layet, and T. Angot, J. Chem. Phys. **134**, 014701 (2011).
[20]D. Haberer, L. Petaccia, Y. Wang, H. Quian, M. Farjam, S. A. Jafari, H. Sachdev, A. V. Federov, D. Usachov, D. V. Vyalikh, X. Liu, O. Vilkov, V. K. Adamchuk, S. Irle, M. Knupfer, B. Büchner, and A. Grüneis, Phys. Status Solidi B **248**, 2639 (2011).
[21]D. Haberer, C. E. Giusca, Y. Wang, H. Sachdev, A. V. Fedorov, M. Farjam, S. A. Jafari, D. V. Vyalikh, D. Usachov, X. Liu, U. Treske, M. Grobosch, O. Vilkov, V. K. Adamchuk, S. Irle, S. R. P. Silva, M. Knupfer, B. Büchner, and A. Grüneis, Adv. Mater. **23**, 4497 (2011).
[22]M. Scheffler, D. Haberer, L. Petaccia, M. Farjam, R. Schlegel, D. Baumann, T. Hänke, A. Grüneis, M. Knupfer, C. Hess, and B. Büchner, ACS Nano **6**, 10590 (2012).
[23]A. Paris, N. Verbitskiy, A. Nefedov, Y. Wang, A. Fedorov, D. Haberer, M. Oehzelt, L. Petaccia, D. Usachov, D. Vyalikh, H. Sachdev, C. Wöll, M. Knupfer, B. Büchner, L. Calliari, L. Yashina, S. Irle, and A. Grüneis, Adv. Funct. Mater. **23**, 1628 (2013).
[24]W. Zhao, J. Gebhardt, F. Späth, K. Gotterbarm, C. Gleichweit, H.-P. Steinrück, A. Görling, and C. Papp, Chem. - Eur. J. **21**, 3347 (2015).
[25]S. Casolo, G. F. Tantardini, and R. Martinazzo, Proc. Natl. Acad. Sci. U. S. A. **110**, 6674 (2013).
[26]L. Hornekær, W. Xu, R. Otero, E. Lægsgaard, and F. Besenbacher, Chem. Phys. Lett. **446**, 237 (2007).
[27]S. Casolo, O. M. Lovvik, R. Martinazzo, and G. F. Tantardini, J. Chem. Phys. **130**, 054704 (2009).
[28]X. Sha, B. Jackson, D. Lemoine, and B. Lepetit, J. Chem. Phys. **122**, 014709 (2005).
[29]J. Kerwin, X. Sha, and B. Jackson, J. Phys. Chem. B **110**, 18811 (2006).
[30]J. Kerwin and B. Jackson, J. Chem. Phys. **128**, 084702 (2008).
[31]S. Morisset, Y. Ferro, and A. Allouche, J. Chem. Phys. **133**, 044508 (2010).
[32]S. Cazaux, S. Morisset, M. Spaans, and A. Allouche, Astron. Astrophys. **535**, A27 (2011).
[33]S. Garashchuk, J. Jakowski, L. Wang, and B. G. Sumpter, J. Chem. Theory Comput. **9**, 5221 (2013).
[34]F. Karlický, B. Lepetit, and D. Lemoine, J. Chem. Phys. **140**, 124702 (2014).
[35]E. R. M. Davidson, J. Klimeš, D. Alfè, and A. Michaelides, ACS Nano **8**, 9905 (2014).
[36]Z. Medina and B. Jackson, J. Chem. Phys. **128**, 114704 (2008).
[37]T. Aizawa, R. Souda, S. Otani, Y. Ishizawa, and C. Oshima, Phys. Rev. B **42**, 11469 (1990).
[38]A. Luntz and J. Harris, Surf. Sci. **258**, 397 (1991).
[39]E. Ghio, L. Mattera, C. Salvo, F. Tommasini, and U. Valbusa, J. Chem. Phys. **73**, 556 (1980).
[40]M. Bonfanti, R. Martinazzo, G. F. Tantardini, and A. Ponti, J. Phys. Chem. C **111**, 5825 (2007).
[41]Y. Wang, H.-J. Qian, K. Morokuma, and S. Irle, J. Phys. Chem. A **116**, 7154 (2012).
[42]E. Vanden-Eijnden and G. Ciccotti, Chem. Phys. Lett. **429**, 310 (2006).
[43]G. A. Worth, M. H. Beck, A. Jäckle, and H.-D. Meyer, The MCTDH package, version 8.2 (2000), H.-D. Meyer, version 8.3 (2002), version 8.4 (2007), version 8.5 (2011), current version 8.5.3 (2013), see http://mctdh.uni-hd.de.
[44]H.-D. Meyer, U. Manthe, and L. S. Cederbaum, Chem. Phys. Lett. **165**, 73 (1990).
[45]M. H. Beck, A. Jäckle, G. A. Worth, and H.-D. Meyer, Phys. Rep. **324**, 1 (2000).
[46]*Multidimensional Quantum Dynamics: MCTDH Theory and Applications*, edited by H.-D. Meyer, F. Gatti, and G. A. Worth (Wiley-VCH, Weinheim, 2009).
[47]Strictly speaking, since the atomistic model is finite, without a true dissipative bath, only *trapping* can occur. The computed probabilities refer to the *plateau* value that they attain in a time window before the onset of the recurrences.
[48]Notice that the strength of the coupling between the probe "H" and the C atom does enter in $J_H(\omega)$ but factors out from the ratio.
[49]A. C. Hewson, *The Kondo Problem to Heavy Fermions* (Cambridge University Press, Cambridge, UK, 1997).
[50]R. Martinazzo, B. Vacchini, K. H. Hughes, and I. Burghardt, J. Chem. Phys. **134**, 011101 (2011).
[51]M. Bonfanti *et al.*, J. Chem. Phys. **143**, 124703 (2015).